PAPER

The influence of laser pulse duration and energy on ICP-MS signal intensity, elemental fractionation, and particle size distribution in NIR fs-LA-ICP-MS

Prasoon K. Diwakar,[*a] Sivanandan S. Harilal,[a] Nicole L. LaHaye,[a] Ahmed Hassanein[a] and Pramod Kulkarni[b]

Laser parameters, typically wavelength, pulse width, irradiance, repetition rate, and pulse energy, are critical parameters which influence the laser ablation process and thereby influence the LA-ICP-MS signal. In recent times, femtosecond laser ablation has gained popularity owing to the reduction in fractionation related issues and improved analytical performance which can provide matrix-independent sampling. The advantage offered by fs-LA is due to shorter pulse duration of the laser as compared to the phonon relaxation time and heat diffusion time. Hence the thermal effects are minimized in fs-LA. Recently, fs-LA-ICP-MS demonstrated improved analytical performance as compared to ns-LA-ICP-MS, but detailed mechanisms and processes are still not clearly understood. Improvement of fs-LA-ICP-MS over ns-LA-ICP-MS elucidates the importance of laser pulse duration and related effects on the ablation process. In this study, we have investigated the influence of laser pulse width (40 fs to 0.3 ns) and energy on LA-ICP-MS signal intensity and repeatability using a brass sample. Experiments were performed in single spot ablation mode as well as rastering ablation mode to monitor the Cu/Zn ratio. The recorded ICP-MS signal was correlated with total particle counts generated during laser ablation as well as particle size distribution. Our results show the importance of pulse width effects in the fs regime that becomes more pronounced when moving from femtosecond to picosecond and nanosecond regimes.

I Introduction

Since the introduction of laser ablation inductively coupled plasma mass spectroscopy (LA-ICP-MS) as a viable analytical method by Gray in 1985,[1] it has become a widely used technique for multi-elemental and isotopic analysis[2] of a variety of solid samples including metals and alloys,[3–5] insulators, glasses,[6] crystals, amorphous materials, plants, biological tissues,[7–10] geological samples, *etc.*[11–14] The important experimental parameters to be optimized in LA-ICP-MS include laser wavelength, laser pulse energy, fluence, pulse duration, pulse repetition rate, spot size, ablation cell design and volume, ablation cell ambient gas properties, gas flow rate, and ICP torch parameters. All these parameters need to be optimized for accurate and precise analysis of the sample. Even after careful optimization of all the parameters, there are certain issues which pose challenges to the technique *viz.* elemental fractionation effect and matrix effects. Elemental fractionation occurs due to preferential ablation of certain elements (low volatility or low vapor pressure elements) present in the sample

resulting in enrichment of one element over the other in laser produced aerosols leading to non-stoichiometric sampling and analysis. This elemental fractionation can occur during different stages of LA-ICP-MS processes including laser ablation stage, aerosol transport, or during atomization and ionization in ICP torch. Matrix effects are related to differences in the response of the system due to the presence or absence of matrix elements in the sample which could alter the signal.

One of the major sources of elemental fractionation is during laser ablation which is the focus of this study. During the ablation process, as a result of the thermal processes, heating of the sample can result in preferential evaporation, melting, and ablation of certain elements from the sample. The laser can also modify the sample matrix or sample composition as a result of thermal effects and therefore, shot to shot variation in the LA-ICP-MS signal can be observed. Thermal effects can result in preferential enrichment or depletion of aerosols generated during the ablation process. Such an effect can be reduced or minimized by lessening laser-induced thermal effects on the sample. Ultra-short laser pulses with pulse durations shorter than the timescales required for heat diffusion to occur in the sample lattice can minimize fractionation effects. Elimination of fractionation and matrix effects can lead to development of a non-matrix matched based calibration system which can be

aCenter for Materials Under Extreme Environment, School of Nuclear Engineering, Purdue University, West Lafayette, IN 47907, USA. E-mail: pdiwakar@purdue.edu
bNational Institute of Occupational Safety and Health, Cincinnati, OH 45213, USA

universally applied to different systems in a variety of operating conditions. With the advent and development of femtosecond laser systems, fs-LA-ICP-MS provides an opportunity to develop a non-matrix matched based calibration system which has been the goal of the LA-ICP-MS community in recent years as is evident from numerous publications and reviews dedicated to understanding this phenomenon.[12,15–21] As described by Garcia *et al.* in a recent review, three steps are required for achieving an ideal LA-ICP-MS system:[16]

1. Formation of aerosols with the same stoichiometry as the sample during the ablation process including no re-deposition of material on the surface,

2. No loss of particles during the transportation stage,

3. Complete atomization and ionization of the aerosols in the ICP.

The reduction of elemental fractionation is largely dependent on experimental conditions which require better understanding of the laser ablation processes and measurement of online particle generation and particle size distribution.

Ablation mechanisms using femtosecond lasers have been studied by different groups in recent times, but the fundamental processes are still not completely understood and the results are controversial.[19,22,23] For fs LA, an intense laser beam is focused onto the sample surface (sometimes a defocused beam is also used for LA-ICP-MS) where the laser pulse energy transfer takes place in two steps. In the first step, photons are absorbed on the surface layer and single or multiphoton ionization processes occur which excite the electrons during first few fs of the laser pulse. In the second step, the absorbed energy is transferred to the lattice by electron–phonon coupling leading to thermal vaporization of the sample which occurs in a few 100 fs–ps time scales (strong ablation) or excited electrons can pull out heavy atoms and ions when they move out resulting in soft ablation. Both modes of the ablation mechanism can occur simultaneously and mechanisms will depend on laser intensities and sample ablation thresholds. In either case, the ablation occurs in ps time durations resulting in explosion like removal of electrons from the sample followed by ion removal. The shape of the fs laser ablation plume is typically forward biased, which avoids re-deposition of the material on the sample surface.[24,25] It is important to minimize material re-deposition on the surface as air flow is least on the surface, so if any material is deposited on the surface, it will not be transported to ICP affecting accuracy and precision of measurement. Studies have shown that using helium as the carrier gas can help in reduction of melt re-deposition on the surface.[26]

There are multiple parameters which can affect the laser ablation process and in turn affect formation of laser produced aerosols. In this study, the focus is on understanding the effect of the laser pulse duration on the LA-ICP-MS signal response, particle size distribution, and particle size induced fractionation effect. Laser pulse width has not been an extensively investigated parameter, especially in the fs regime, owing to complications in modifying the pulse width in commercial femtosecond laser systems. There have been few studies on natural Monazite as a sample which focused on the effect of laser pulse width on the ICP-MS signal.[27–29] They did not find
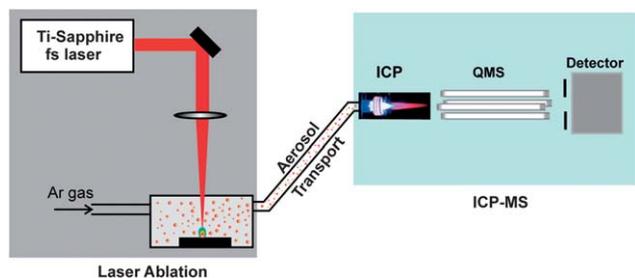
any significant effect of pulse width on LA-ICP-MS performance, although a maximum ICP-MS signal intensity was observed for 200 fs pulse width as opposed to the shortest pulse width studied. Chien and Gupta[30] studied the effect of pulse width on ultra-fast laser processing of materials and observed thermal effects at 2.5 ps for stainless steel. The fundamental aspects are still not clear and further research is required to understand the role of pulse width in ablation efficiency, particle formation, particle size distribution, particle induced fractionation effects, *etc.*

Various studies have been conducted to understand the role of particle size distribution in elemental fractionation for both ns and fs-LA-ICP-MS using different types of techniques.[31–40] In general, it has been shown that smaller sized particles or soft agglomerates reduce fractionation due to complete ionization of the particles in ICP. Large particles result in incomplete ionization as well as spiky signal response. Nanosecond laser ablation has been shown to result in generation of a bimodal distribution of particle size while femtosecond laser ablation has been shown to result in generation of unimodal distribution with peak diameters ranging between 10 nm and 100 nm.[41,42] Even with small sized particles, preferential melting and vaporization can occur which could result in production of aerosols, which are not representative of the sample.

We have systematically studied the effect of fs laser pulse width on particle size induced elemental fractionation using a brass sample which is known to show severe elemental fractionation effects owing to differences in volatilities of Cu and Zn. For particle size measurements, a Differential Mobility Analyzer (DMA) combined with a Condensation Particle Counter (CPC) was used which provides the mobility diameter of the particle. It is important to note that the DMA does not see the physical particles rather measures their mobility based on electrical and physical properties of the particles as well as the flow conditions. Therefore, individual particles and agglomerates of small particles with similar overall dimensions will be measured as the same particle mobility diameter. Additionally, particle shape, size, and morphology can influence the measured mobility diameter using the DMA.[35,40] Even with these limitations, a DMA combined with a CPC offers valuable information regarding particle size distribution and gives an opportunity to conduct online particle size measurements as well as selectively introduce particles of specific sizes to the ICP to understand particle size induced elemental fractionation.

II Experimental

Fig. 1 shows the schematic of the experimental setup. It consists of a laser ablation unit, aerosol transportation tube and ICP-MS for elemental analysis. A femtosecond Ti:sapphire laser system (Amplitude Technologies) operating at 800 nm wavelength and 10 Hz frequency was used in this study which works on the chirped-pulse amplification (CPA) technique. The maximum rated output of the laser was 10 mJ, though only energies between 20 and 800 μJ were used for the experiments reported in the present study. Laser pulse energy variation was below 2% while contrast was of the order of 10^{-7}. Low contrast ensures

This journal is © The Royal Society of Chemistry 2013

J. Anal. At. Spectrom., 2013, **28**, 1420–1429 | **1421**

Fig. 1 Schematic of the experimental setup. A Ti-sapphire fs laser is used for ablation. The ablated particles are transported to the ICP torch for atomization and ionization using Ar as the carrier gas (QMS: quadruple mass spectrometer).

Table 1 Summary of important laser, samples, and ICP-MS parameters for 800 nm fs-LA-ICP-MS

Experimental parameters	
Laser system/beam delivery	
Wavelength/pulse duration	800 nm, 40 fs to 300 ps
Energy	20–800 μJ
Repetition rate	10 Hz
Beam diameter	10 mm
Spot size	~100 μm
Fluence	0.25–10 J cm^{-2}
Angle of incidence	Normal to the target
Objective lens NA	0.13
Sampling mode	Single spot and raster
ICP-MS	
Torch RF power	1550 W
Carrier gas	1.0 L min^{-1} Ar
Gas through torch	15 L min^{-1} Ar
Integration time per isotope	10 ms
Dwell time	150 ms
Data acquisition mode	Time resolved (TRA)
Sample material	
Brass	Cu 64% (boiling temperature 2576 °C), Zn 33% by weight (boiling temperature 907 °C)
Isotopes analyzed	^{63}Cu, ^{65}Cu, ^{64}Zn, ^{66}Zn, ^{67}Zn, ^{68}Zn

that no pre- or post-nanosecond pulse is present in the laser pulse output. The pulse duration of the femtosecond laser pulse was changed by adjusting the compressor optics. Using this system, the laser pulse width can be varied from 40 fs to 1.2 ps. The pulse width was measured using an auto-correlator which was developed in-house. For 300 ps, the laser beam was tapped before the compressor. Energy of the laser pulses was attenuated using a combination of a half-wave plate and a thin film polarizer positioned before the compressor optics. Laser beam was diverted to the ablation chamber (J100 Series, Applied Spectra) using a set of mirrors and finally was focused in the ablation chamber using an objective lens. The spot size on the sample was kept constant at ~100 μm. The ablation chamber was mounted on an *XYZ* translation stage which facilitated the movement of the sample. Rastering as well as the same spot ablation modes were used in this study. For the same spot ablation mode, the stage was kept fixed at one location while for the rastering mode, the stage traversed in *X* and *Y* directions at a pre-defined constant speed of ~50 μm s^{-1}. High purity Ar gas was used in the ablation cell at a constant flow rate of 1.0 L min^{-1} to flush out the laser-produced aerosols. The ablation chamber was thereby connected to the ICP-MS system (Agilent Technologies Inc., ICP-MS 7700×) using Tygon tubing.

Brass (Goodfellow, USA) was chosen as a sample for this study because of known elemental fractionation issues with brass using ICP systems as well as extensive studies conducted on brass by other research groups. Six different isotopes were analyzed: ^{63}Cu, ^{65}Cu, ^{64}Zn, ^{66}Zn, ^{67}Zn, ^{68}Zn. It is important to note that the primary goal of this work was to study the trend of the elemental ratio of Cu and Zn with different laser pulse widths and particle sizes and not to evaluate the exact elemental ratio, which will be dependent on multiple operating parameters. ICP-MS measurements were performed in transient analysis mode with an integration time of 10 ms for each isotope. Laser ablation was initiated 10 seconds after the gas blank measurement. Acquisition time (time resolved analysis, TRA) was set to ~150 seconds which included ~90 seconds of ablation followed by ~60 seconds of wash out time. ICP-MS was tuned to maximize sensitivity before start of each experiment. Particle size distributions were obtained using a differential mobility analyzer (DMA) (TSI 3080) and a condensation particle counter (CPC) (TSI 3022A) which was connected in between the LA chamber and ICP-MS. The sheath flow of the DMA was set to

10 L min^{-1}. With this sheath flow and voltage range, the DMA was able to generate monodisperse particles with diameters of 50–317 nm. Total particle counts were also obtained using the CPC alone. Table 1 lists the important experimental operating conditions used in this study.

III Results and discussion

(a) The effect of laser pulse duration

ICP-MS signal intensity was monitored for various laser pulse widths. Fig. 2 shows the effect of femtosecond laser pulse width on the transient ICP-MS signal intensity. The ^{63}Cu isotope
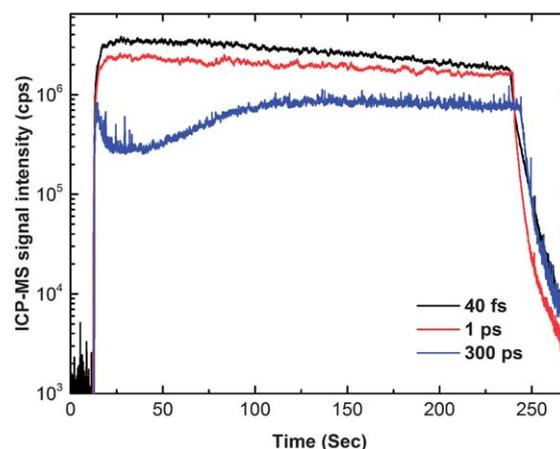

Fig. 2 Effect of laser pulse width on the transient ICP-MS signal. A laser fluence of 1.5 J cm^{-2} was used in the same spot ablation mode. The corresponding laser irradiances were 6.7×10^{14} W cm^{-2}, 1.5×10^{12} W cm^{-2}, and 5×10^{9} W cm^{-2} for 40 fs, 1 ps, and 300 ps pulses respectively.

ICP-MS signal is shown for three different pulse widths (40 fs, 1 ps and 300 ps) with a laser fluence of 1.5 J cm^{-2}. It can be seen that there is no significant effect on the ICP-MS temporal signal for pulse widths in the femtosecond regime (40 fs and 1 ps), although the signal intensity is lower for the 1 ps case which can be attributed to the decrease in irradiance as well as possible plasma shielding for 1 ps. For the 300 ps case, which can effectively be considered in the nanosecond regime, the signal considerably decreases by one order of magnitude. The difference in signal intensity between 40 fs and 300 ps can be attributed to the reduction of laser irradiance when fluence is kept constant resulting in a much decreased ablation efficiency.

Particle size distribution can also play an important role in the ICP-MS signal intensity. For the fs regime, it has been shown that smaller sized particles are generated which are easier to ionize and decompose in ICP resulting in higher signals as compared to ns pulses which can result in generation of larger sized particles.[4,33] The increase in the signal for the 40 fs pulse can also be due to the increase in the number of small particles or soft agglomerates which are completely ionized in ICP, maximizing the signal intensity. It is interesting to note the differences in the trend of transient signals for fs pulses and 300 ps laser pulse. As ablation proceeds, the decrease in the 300 ps signal is drastic which could occur due to a combination of effects including reduced irradiance, crater effects and thermal induced effects. Also it should be noted that the ablation mechanisms are entirely different for fs and ns LA which can lead to different transient signal trends. The presence of spikes in the 300 ps laser pulse shows that aerosols with large particle size diameters are generated, especially during early times of ablation. The ICP signal stabilizes after 150 seconds of ablation (~1500 laser shots). Freydier et al.[11] showed a similar trend in transient ICP-MS signal for different pulse widths ranging from 60 fs to 3 ps, though a fluence of 10 J cm^{-2} was used in their study, which is considerably higher as compared to the current study.
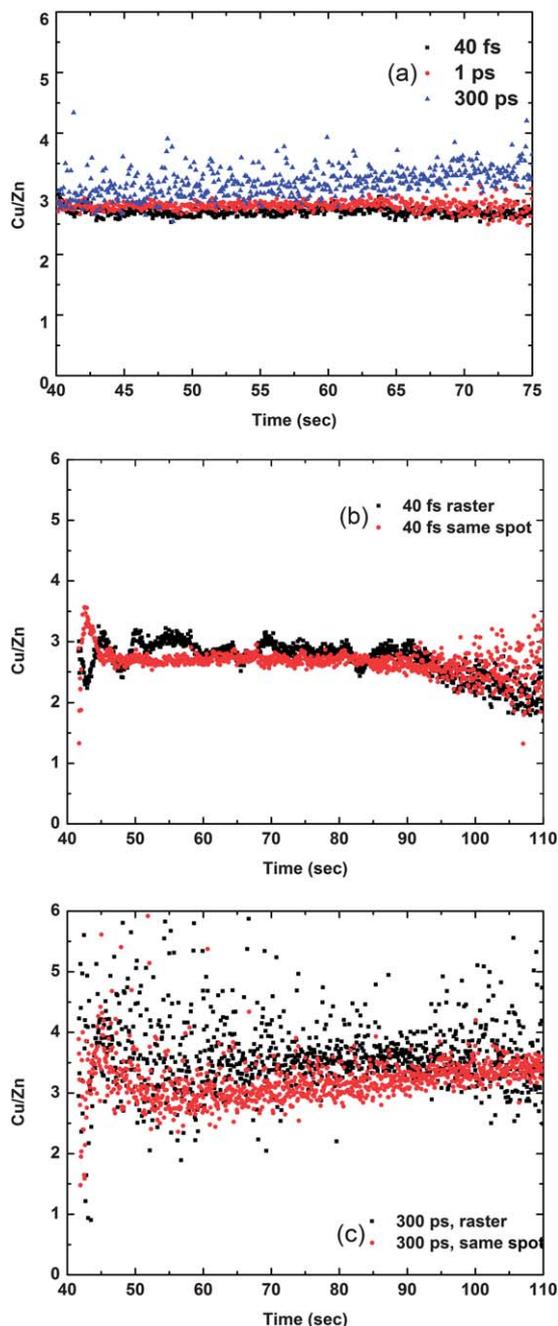
Fig. 3 compares the effect of rastering vs. single spot ablation modes for different laser pulse widths on transient ICP-MS signal intensity. It can be clearly seen that there is no significant difference in raw counts of ^{63}Cu isotope for either rastering or scanning mode for the fs regime which signifies that both the raster mode and the same spot mode can yield repeatable results. In the 300 ps case, the difference can be seen in the trend of the transient signal, which can be attributed to crater as well as thermal effects. Rastering mode results in a consistent level of signal for all the pulse widths studied in the fs regime. However, for the 300 ps case signal intensity is higher for rastering as compared to the single spot mode. This difference can be due to the crater effect. For longer pulse widths and for single spot ablation, the laser-target and laser plasma coupling can be affected by crater depth. The signal decays initially followed by an increase as the ablation progresses on the single spot. The increase in signal could be due to re-heating and melting of the deposited matter on the walls and boundaries of crater and on the sample surface.

Fig. 4 shows the effect of pulse width and ablation mode (single spot vs. raster) on elemental ratio (Cu/Zn) which is important for understanding the role of these parameters in elemental fractionation. It can be clearly seen that the fs regime
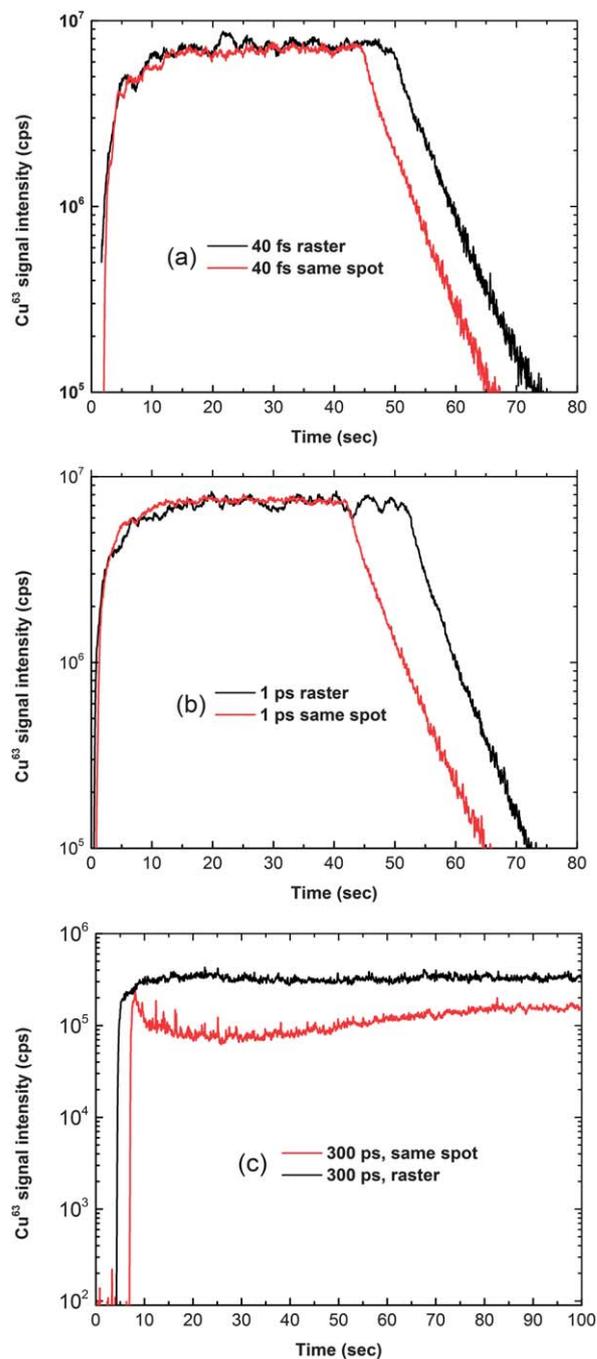
Fig. 3 Effects of different laser pulse widths and sampling modes (rastering vs. same spot) on the ICP-MS signal are given. A laser fluence of 1.5 J cm^{-2} was used in this study. For the rastering experiments, the brass sample was moved under the stationary laser beam at ~50 μm s^{-1}. The laser pulse widths used were (a) 40 fs, (b) 1 ps, and (c) 300 ps.

results in less dispersion of elemental ratio; least dispersion is observed for the 40 fs laser pulse. Also the elemental ratio is very steady for the duration of ablation. For the 1 ps case, there is a slight increase in the elemental ratio; this increase is significantly enhanced for the 300 ps case. The 1 ps pulse duration is fairly comparable to the electron–phonon coupling time scale, which could alter the chemical composition of aerosols due to elemental fractionation. Additionally, for the same fluence,
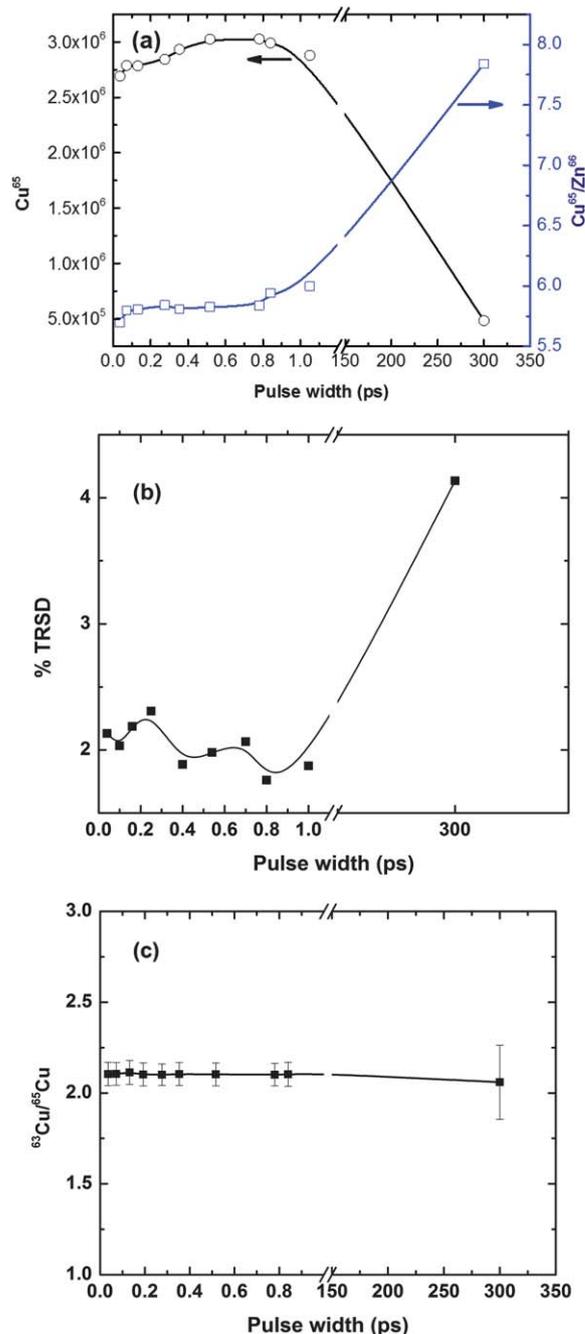
rastering mode (Fig. 4b and c). In the rastering mode, material from the top surface is removed which might not be representative of the bulk sample because of contamination and oxidation of the surface, possibly resulting in slightly different Cu/Zn ratio than the bulk.

Fig. 5 shows the effect of pulse width, ranging from 40 fs to 300 ps, on ICP-MS signal counts, elemental ratios of Cu and Zn transient relative standard deviation (TRSD[43]) and isotopic ratio of ^{63}Cu and ^{65}Cu. Overall, the pulse width did not influence the

Fig. 4 (a) The effect of pulse width on elemental ratio is given. The Cu/Zn ratios obtained for single spot and rastering ablation modes are given for (b) 40 fs and (c) 300 ps. The laser fluence used for the measurement was 1.5 J cm^{-2}. For rastering experiments, the brass sample was moved under the stationary laser beam at ~50 μm s^{-1}.
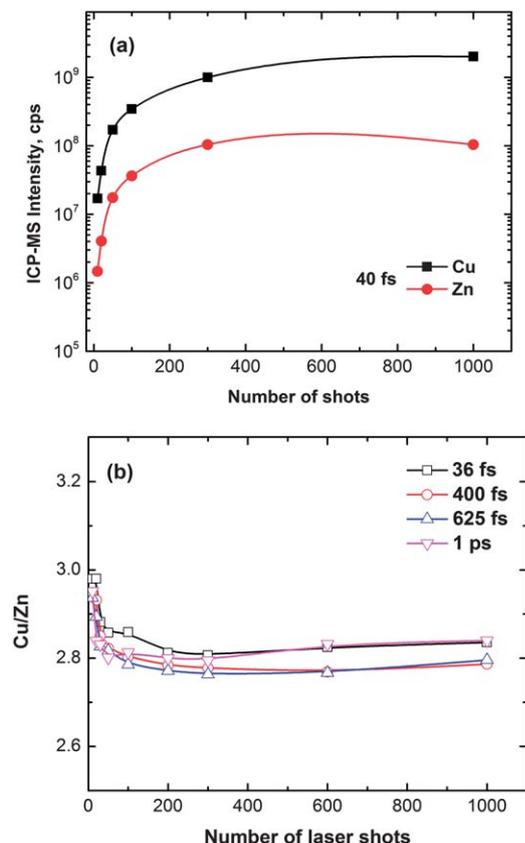
irradiance decreases to ~10^{12} W cm^{-2} for 1 ps, which could change the ionization and ablation mechanism and thereby affect particle formation processes. For the 300 ps case, the fractionation effect can be easily understood and correlated with thermal effects and formation of bigger particles which are preferentially loaded with Cu as has been shown in earlier studies.[16,33] The same spot ablation resulted in more repeatable Cu/Zn ratios for all the pulse widths as compared to the

Fig. 5 (a) The effects of pulse width on ICP-MS signal intensity and elemental ratio are given. The effects of pulse width on TRSD and isotopic ratios are shown in (b) and (c) respectively. Optimized conditions were achieved for the 400–600 fs pulse width. The laser fluence used for the measurements was 1.5 J cm^{-2}.

1424 | J. Anal. At. Spectrom., 2013, **28**, 1420–1429

This journal is © The Royal Society of Chemistry 2013

Fig. 6 Role of the number of laser shots in (a) Cu and Zn signal intensity for the 40 fs laser pulse and (b) elemental ratio for different laser pulse widths, with a laser fluence of 1.5 J cm^{-2} for both plots.

elemental ratios as well as isotopic ratios significantly in the femtosecond regime, although optimized and accurate elemental ratios were obtained for 400–600 fs. The ICP-MS signal was maximum and TRSD was minimum for 400–600 fs. Poitrasson et al.[28] observed a similar trend that the maximum ICP-MS signal intensity was found for 200 fs as compared to the shortest pulse width studied.

We also evaluated the number of laser shots necessary for obtaining accurate elemental ratios. The maximum observed ICP-MS signal intensity for various numbers of 40 fs laser shots is given in Fig. 6 along with the Cu/Zn ratio for various pulse widths and number of shots. As expected, the Cu and Zn signal intensity increases with the number of shots and then reaches a steady value after a few hundred shots. The general trend is the same for all the laser pulse widths studied, i.e., for first initial shots the elemental ratio is higher than expected and then approaches a steady value after a few tens of shots. 400–600 fs pulses resulted in better elemental ratios. These results highlight that, for single spot ablation, less than 10 shots are necessary when using fs pulses at 800 nm for stoichiometric determination of bulk and thin samples.

(b) Role of laser pulse energy

The characteristics of laser ablation and particle generation are strongly dependent on the deposited energy at the target

surface. For a given laser pulse width, the change in laser energy affects both laser-target and laser-plasma coupling. We compared the elemental ratios and TRSD for 40 fs and 300 ps pulse widths and the results are given in Fig. 7. Large deviations from expected elemental ratios are observed for both 40 fs and 300 ps pulse widths at lower energies. However, laser pulse energies above ~100 μJ (fluence ~ 1.25 J cm^{-2}) resulted in the expected elemental ratio for the 40 fs case, while for 300 ps, the ratio varied considerably with energy and a stable operating range was not observed. For 40 fs pulses and at lower energies (<100 μJ, fluence < 1.25 J cm^{-2}), only particles from the top layer of the brass sample are ablated which might not be representative of the bulk sample resulting in an erroneous Cu/Zn ratio. As energy is increased the Cu/Zn ratio shows asymptotic behavior and approaches a stable value with minimum TRSD (<2%). For 300 ps, no such asymptotic behavior is reached though reasonable elemental values are observed at higher laser energy levels (≥250 μJ). Gamaly et al.[44] showed that the laser ablation threshold is nearly constant for pulse widths ≤ 1 ps (e.g., ablation threshold for Cu ~0.51 J cm^{-2}) and the threshold for ablation varies as a function of pulse width (τ) in the picosecond or nanosecond regime (ablation threshold as 0.045 J cm$^{-2} \times \sqrt{\tau}$ (ps)). The TRSD is also found to vary with respect to laser energy and for 40 fs FWHM, the minimum RSD
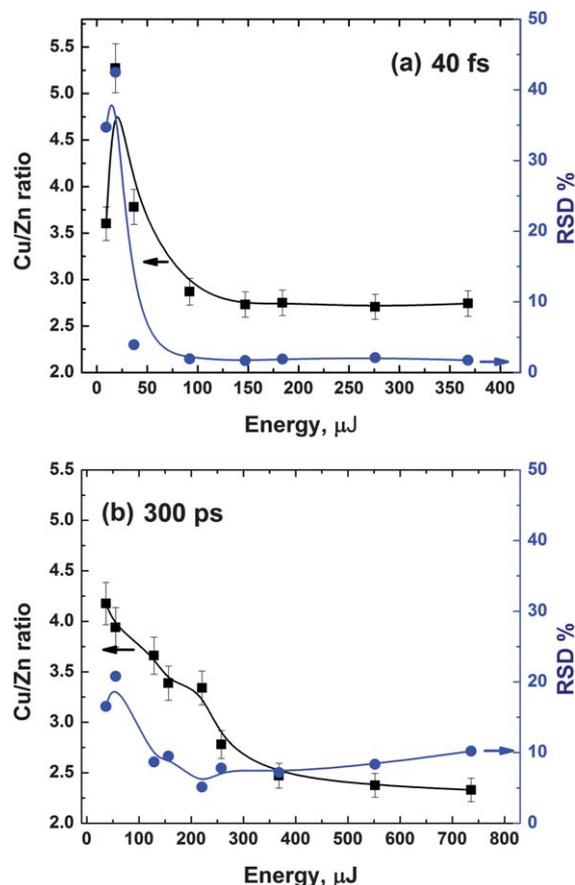
Fig. 7 Effect of laser pulse energy on elemental ratio and transient RSD for (a) 40 fs and (b) 300 ps pulse widths.
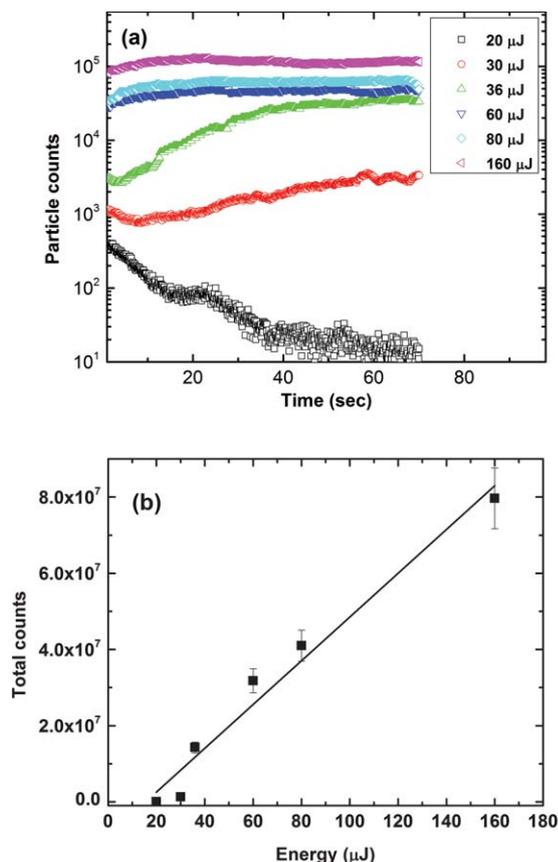
This journal is © The Royal Society of Chemistry 2013

J. Anal. At. Spectrom., 2013, 28, 1420–1429 | 1425

Fig. 8 Effect of laser pulse energy on the total number of particles generated for the 40 fs laser pulse: (a) transient mode and (b) total sum of particles.

is noticed at laser energies where the expected elemental ratios are obtained. However, for 300 ps laser ablation, the TRSDs are found to be significantly higher irrespective of the laser energy used compared to shorter pulse laser ablation.

The elemental ratio as well as RSD showed significant variation with respect to laser energy. It is interesting to observe the number of total particles generated during ablation as a function of ablation time for various laser energy levels. Laser produced brass aerosols were directly transported to CPC for measurement of the total number of particles generated. Fig. 8(a) shows the particle counts for different laser pulse energies at 40 fs laser pulse width. For the lowest laser pulse energy studied (20 μJ), the particle counts continuously decrease as the ablation progresses. The ablation phenomenon at this irradiance is very close to the ablation threshold and after the first few particles are ablated from the surface due to desorption, laser pulse is unable to ablate further material leading to a decrease in particle number counts. As the laser pulse energy is increased beyond the ablation threshold, the ablation mechanism is different and particle generation increases. At higher energies beyond 60 μJ, steady numbers of particles are generated for the duration of acquisition lasting about 70 seconds. There is a linear increase in the total number of particles generated with laser pulse energy above ablation threshold as shown in Fig. 8(b).

(c) Particle density and size distribution

It has been articulated that elemental fractionation in LA-ICP-MS is directly related to particle size distribution. Smaller sized particles or soft agglomerates reduce fractionation due to complete ionization of the particles in ICP, while incomplete ionization of large particles leads to fractionation along with spiky signal behavior. Fig. 9 shows the effect of the laser pulse width on total particle counts and time dependent changes for a fixed laser pulse energy of 120 μJ. The general trend is similar for all the studied laser pulse widths with an increase in particle counts initially followed by a gentle decrease as the crater depth increases. Interestingly, the particle counts are the lowest for 40 fs and maximum in the range of 400–600 fs pulse widths. This is also evident in the ICP-MS signal where the maximum counts are observed for 400–600 fs pulse widths. It may be possible that 40 fs results in generation of a large number of small sized particles loosely held together to form soft agglomerates which can decrease the total particle counts as measured by CPC. Additionally, some smaller particles can also be lost *via* diffusion in the transport tube and thereby lead to a reduced number of particles reaching CPC. When comparing 40 fs with 1 ps, it can be seen that even though the number of counts for 40 fs is lower than 1 ps, the ICP-MS signal is higher for the 40 fs case which may be possible if fs ablation results in the formation of soft agglomerates consisting of very fine
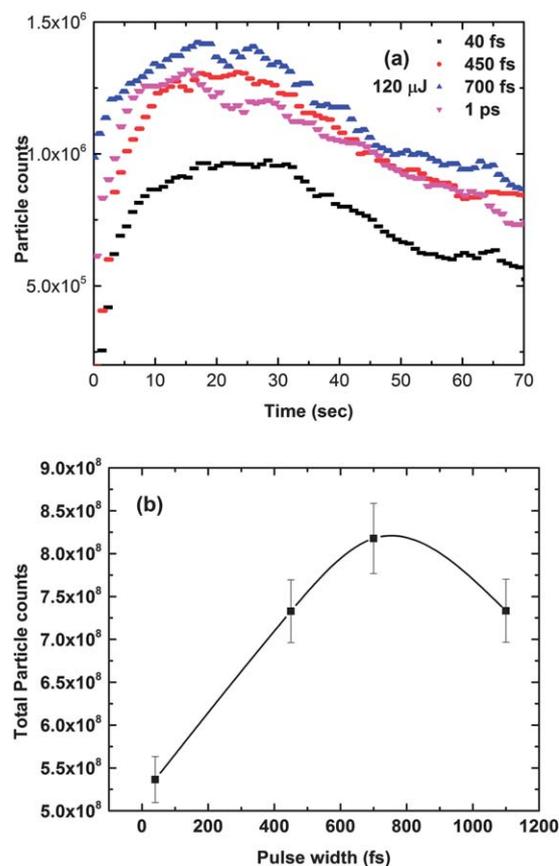

**Fig. 9** Effect of laser pulse width on the total detectable number of particles: (a) transient mode and (b) total sum of particles.

1426 | *J. Anal. At. Spectrom.*, 2013, **28**, 1420–1429

This journal is © The Royal Society of Chemistry 2013

Paper

JAAS

particles resulting in better ionization of the aerosols in the ICP torch enhancing the signal intensity.[36,38]

We also investigated the role of pulse width and laser energy in particle size distribution. Particle distribution shown for 120 μJ in Fig. 10(a) shows that pulse width affects particle number density while the distribution remains unchanged. Normalized particle counts as shown in Fig. 10(b) show that the peak mean particle diameter changes from ~100 nm to ~140 nm by changing the energy from 40 μJ to 160 μJ. It indicates that laser pulse energy affects distribution as well as the particle number density. Increased irradiance results in an increase in number density. In the femtosecond regime, a large number of small sized particles are formed which could enhance particle collisions forming agglomerates with larger effective diameters.

A DMA combined with a CPC was used to select particles/agglomerates of specific size for introduction in the ICP-MS system to understand particle size induced elemental fractionation. Fig. 11(a) shows that for a 40 fs laser pulse at 120 μJ, elemental fractionation does occur and is dependent on the particle/agglomerate size. Small particles (<50 nm) have been shown to mainly consist of single individual particles consisting mainly of highly volatile elements of the sample which in this
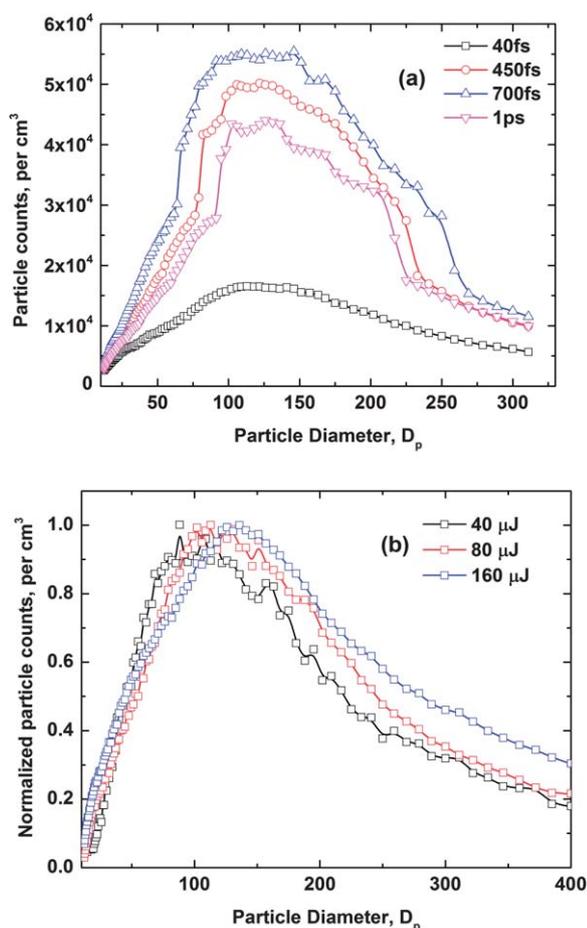
Fig. 10 (a) Pulse width did not affect the particle size distribution (mode ~ 100 nm). (b) Increase in laser pulse energy shifted the particle size distribution towards a larger particle size.
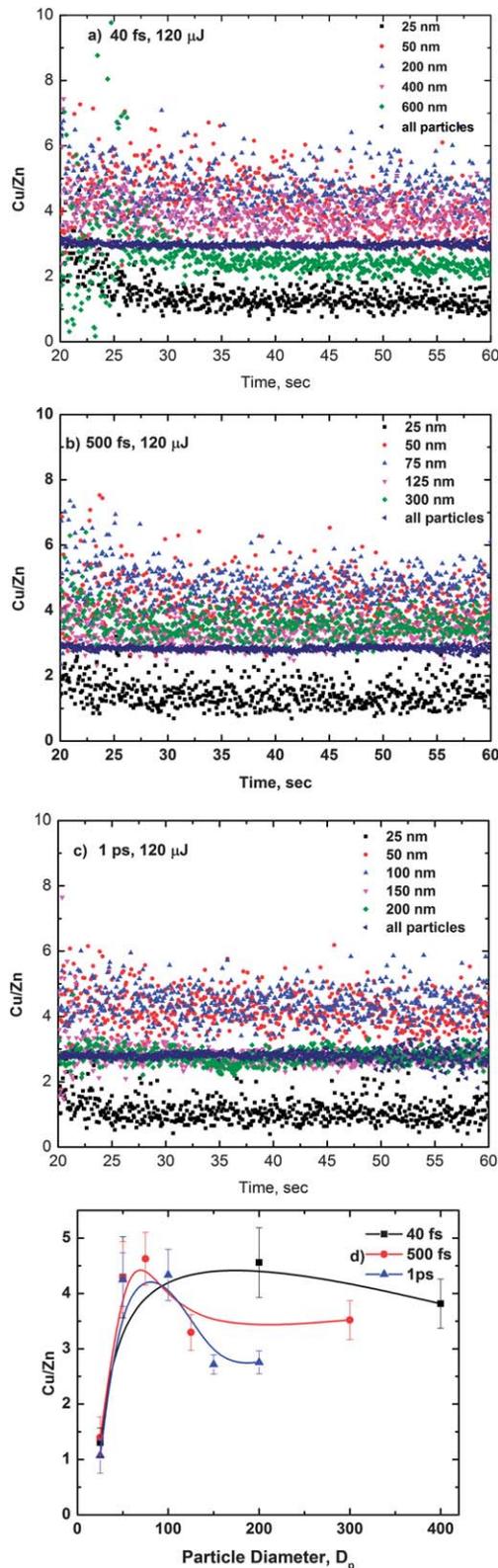
Fig. 11 Effect of particle size on elemental ratio as measured using the ICP-MS system. (a) 40 fs, (b) 500 fs, and (c) 1 ps. (d) Average Cu/Zn with standard deviation for different particle sizes.

This journal is © The Royal Society of Chemistry 2013

J. Anal. At. Spectrom., 2013, **28**, 1420–1429 | **1427**

study is Zn. It is clearly seen that for all the pulse widths in the femtosecond regime, small particles are enriched in zinc. For larger particles (>50 nm), it is possible that they can be either individual particles or spheres or agglomerates of smaller particles. In the first case, they are typically enriched in Cu as has been shown by other studies which explain higher Cu/Zn.[33,41] In the second case, Zn should be enriched which would bring down the ratio as is evident in Fig. 11(a–d). In general, it is shown here that elemental fractionation does exist and is dependent on particle size for femtosecond laser ablation. It is important to note that by selecting particles of a specific size, the mass loading was reduced in ICP which could further induce fractionation effects as with high mass loading, high ionization energy elements like Zn will be inefficiently ionized resulting in fractionation effects.[45] Further investigations are currently in progress to understand the details of the elemental fractionation observed and the relationship with particle size and mass loading effects.

IV   Conclusions

The role of laser pulse width ranging from 40 fs to 0.3 ns, ablation modes (rastering *vs.* scanning), and energy in LA-ICP-MS signal intensity, particle size distribution, and elemental fractionation was studied for a better understanding of fs-LA-ICP-MS signals. No significant pulse width effect was observed on the LA-ICP-MS elemental ratio for fs pulse-widths ranging from 40 fs to 1 ps for the same spot ablation mode, although 400–600 fs resulted in better figures of merit in terms of better RSD, signal intensity, and particle generation. The 300 ps laser ablation showed considerable fractionation effects as indicated by deviation from the Cu/Zn ratio. The presence of spikes in the 300 ps ICP-MS signal showed that the aerosols with large particle sizes were generated during early times of the ablation. Signal intensity was higher for fs pulses compared to picosecond pulses. The increase in signal for fs pulses can be attributed to the increase in laser irradiance as well as generation of fine aerosol particles or agglomerates which could result in improved ionization of the aerosols in the ICP torch.

Femtosecond pulses, in general, showed less dispersion of elemental ratio, with 40 fs showing the least dispersion. Single spot mode showed better stability and accuracy in the Cu/Zn ratio as compared to rastering mode. In single spot mode, the signal showed an increase with the number of shots and then approached a steady value. Elemental ratio also approached a steady value after a few tens of laser shots which show that only a few shots are required for stoichiometric ablation of the sample signifying the importance of fs LA-ICP-MS in thin film analysis. For the 40 fs pulse width, elemental ratio showed an asymptotic trend with laser pulse energy approaching a stable ratio for laser pulse energy higher than 100 μJ. While for a 300 ps laser pulse width no such asymptotic behavior was observed. Pulse width influenced particle number density while the distribution remains unchanged. Laser pulse energy affected both the distribution as well as the particle number density. The mean peak particle/agglomerate diameter changed from ∼100 nm to ∼140 nm with increasing energy from 40 μJ to 160 μJ which could be attributed to the increase in particle generation and possible enhanced agglomeration for higher laser pulse energy.

A DMA in combination with a CPC allowed online measurements and introduction of particles of selected size into the ICP-MS system provided better understanding of particle size induced elemental fractionation effects occurring during laser ablation as well as during ICP. Significant particle size based elemental fractionation was observed for all the pulse widths including femtosecond laser pulses. Smaller particles (∼25 nm) showed enrichment in Zn while larger particles showed enrichment in copper which could be due to the combination of mass loading effects as well as particle induced fractionation effects, which requires further investigation.

Acknowledgements

References

1 A. L. Gray, *Analyst*, 1985, **110**, 551–556.
2 J. S. Becker, *J. Anal. At. Spectrom.*, 2002, **17**, 1186–1193.
3 H. R. Kuhn and D. Gunther, *Anal. Chem.*, 2003, **75**, 747–753.
4 V. Mozna, J. Pisonero, M. Hola, V. Kanicky and D. Gunther, *J. Anal. At. Spectrom.*, 2006, **21**, 1194–1201.
5 J. Gonzalez, C. Y. Liu, X. L. Mao and R. E. Russo, *J. Anal. At. Spectrom.*, 2004, **19**, 1165–1168.
6 M. Walle, J. Koch and D. Gunther, *J. Anal. At. Spectrom.*, 2008, **23**, 1285–1289.
7 J. S. Becker, M. Zoriy, J. S. Becker, J. Dobrowolska and A. Matusch, *J. Anal. At. Spectrom.*, 2007, **22**, 736–744.
8 J. S. Becker, M. Zoriy, M. Przybylski and J. S. Becker, *J. Anal. At. Spectrom.*, 2007, **22**, 63–68.
9 M. V. Zoriy and J. S. Becker, *Int. J. Mass Spectrom.*, 2007, **264**, 175–180.
10 H. Sela, Z. Karpas, M. Zoriy, C. Pickhardt and J. S. Becker, *Int. J. Mass Spectrom.*, 2007, **261**, 199–207.
11 R. Freydier, F. Candaudap, F. Poitrasson, A. Arbouet, B. Chatel and B. Dupre, *J. Anal. At. Spectrom.*, 2008, **23**, 702–710.
12 B. Fernandez, F. Claverie, C. Pecheyran and O. F. X. Donard, *TrAC, Trends Anal. Chem.*, 2007, **26**, 951–966.
13 D. Gunther, R. Frischknecht, C. A. Heinrich and H. J. Kahlert, *J. Anal. At. Spectrom.*, 1997, **12**, 939–944.
14 K. E. Jarvis and J. G. Williams, *Chem. Geol.*, 1993, **106**, 251–262.
15 R. E. Russo, X. L. Mao, J. J. Gonzalez and S. S. Mao, *J. Anal. At. Spectrom.*, 2002, **17**, 1072–1075.
16 C. C. Garcia, H. Lindner and K. Niemax, *J. Anal. At. Spectrom.*, 2009, **24**, 14–26.
17 J. Gonzalez, S. H. Dundas, C. Y. Liu, X. L. Mao and R. E. Russo, *J. Anal. At. Spectrom.*, 2006, **21**, 778–784.
18 R. E. Russo, X. L. Mao, C. Liu and J. Gonzalez, *J. Anal. At. Spectrom.*, 2004, **19**, 1084–1089.

19 L. Jiang and H. L. Tsai, in *Proceedings of NSFWorkshop on Research Needs in Thermal, Aspects of Material Removal*, Author Anonymous, Stillwater, OK, 2003.

20 Q. Z. Bian, C. C. Garcia, J. Koch and K. Niemax, *J. Anal. At. Spectrom.*, 2006, **21**, 187–191.

21 J. Koch and D. Gunther, *Anal. Bioanal. Chem.*, 2007, **387**, 149–153.

22 E. G. Gamaly, A. V. Rode, B. Luther-Davies and V. T. Tikhonchuk, *Phys. Plasmas*, 2002, **9**, 949–957.

23 E. G. Gamaly, A. V. Rode, V. T. Tikhonchuk and B. Luther-Davies, *Appl. Surf. Sci.*, 2002, **197**, 699–704.

24 J. Koch, S. Schlamp, T. Rosgen, D. Fliegel and D. Gunther, *Spectrochim. Acta, Part B*, 2007, **62**, 20–29.

25 B. Verhoff, S. S. Harilal, J. R. Freeman, P. K. Diwakar and A. Hassanein, *J. Appl. Phys.*, 2012, **112**, 093303.

26 S. M. Eggins, L. P. J. Kinsley and J. M. G. Shelley, *Appl. Surf. Sci.*, 1998, **127**, 278–286.

27 F. X. d'Abzac, F. Poitrasson, R. Freydier and A. M. Seydoux-Guillaume, *J. Anal. At. Spectrom.*, 2010, **25**, 681–689.

28 F. X. d'Abzac, A. M. Seydoux-Guillaume, J. Chmeleff, L. Datas and F. Poitrasson, *Spectrochim. Acta, Part B*, 2011, **66**, 671–680.

29 F. X. D'Abzac, A. M. Seydoux-Guillaume, J. Chmeleff, L. Datas and F. Poitrasson, *J. Anal. At. Spectrom.*, 2012, **27**, 99–107.

30 C. Y. Chien and M. C. Gupta, *Appl. Phys. A: Mater. Sci. Process.*, 2005, **81**, 1257–1263.

31 C. Liu, X. L. Mao, S. S. Mao, X. Zeng, R. Greif and R. E. Russo, *Anal. Chem.*, 2004, **76**, 379–383.

32 H. R. Kuhn, J. Koch, R. Hargenroder, K. Niemax, M. Kalberer and D. Gunther, *J. Anal. At. Spectrom.*, 2005, **20**, 894–900.

33 J. Koch, A. von Bohlen, R. Hergenroder and K. Niemax, *J. Anal. At. Spectrom.*, 2004, **19**, 267–272.

34 M. Guillong and D. Gunther, *J. Anal. At. Spectrom.*, 2002, **17**, 831–837.

35 N. J. Saetveit, S. J. Bajic, D. P. Baldwin and R. S. Houk, *J. Anal. At. Spectrom.*, 2008, **23**, 54–61.

36 R. Glaus, R. Kaegi, F. Krumeich and D. Gunther, *Spectrochim. Acta, Part B*, 2010, **65**, 812–822.

37 J. J. Gonzalez, C. Liu, S. B. Wen, X. Mao and R. E. Russo, *Talanta*, 2007, **73**, 577–582.

38 J. J. Gonzalez, C. Y. Liu, S. B. Wen, X. L. Mao and R. E. Russo, *Talanta*, 2007, **73**, 567–576.

39 D. C. Perdian, S. J. Bajic, D. P. Baldwin and R. S. Houk, *J. Anal. At. Spectrom.*, 2008, **23**, 336–341.

40 D. C. Perdian, S. J. Bajic, D. P. Baldwin and R. S. Houk, *J. Anal. At. Spectrom.*, 2008, **23**, 325–335.

41 J. Koch, H. Lindner, A. von Bohlen, R. Hergenroder and K. Niemax, *J. Anal. At. Spectrom.*, 2005, **20**, 901–906.

42 R. Jaworski, E. Hoffmann and H. Stephanowitz, *Int. J. Mass Spectrom.*, 2002, **219**, 373–379.

43 J. J. Gonzalez, A. Fernandez, X. L. Mao and R. E. Russo, *Spectrochim. Acta, Part B*, 2004, **59**, 369–374.

44 A. V. Rode, E. G. Gamaly, B. Luther-Davies, B. T. Taylor, J. Dawes, A. Chan, R. M. Lowe and P. Hannaford, *J. Appl. Phys.*, 2002, **92**, 2153–2158.

45 J. Koch, M. Walle, J. Pisonero and D. Gunther, *J. Anal. At. Spectrom.*, 2006, **21**, 932–940.